REVISITING THE STRUCTURAL SETTING OF THE GLUECKSTADT GRABEN SALT STOCK FAMILY, NORTH GERMAN BASIN

M. Baykulov, H.-J. Brink, D. Gajewski, M.-K. Yoon

email: *mikhail.baykulov@zmaw.de*

keywords: *Common Reflection Surface (CRS) stack, Glueckstadt Graben, North German Basin, reflection tomography*

ABSTRACT

Reprocessing of seismic data of a salt stock family from the North German Basin provided new insights into the structural evolution of this area. The Common Reflection Surface (CRS) stack technique was applied to reprocess the reflection data acquired by the hydrocarbon industry in the 1980s. Due to the low fold of these data and the complex geology in the study area severe imaging challenges were encountered when the data were initially processed using conventional CMP stack. The CRS stack technique is particularly suited for low fold data in complex areas since it builds physically correct super gathers even if dipping structures are present. This leads to a considerably improved signal-to-noise ratio in the CRS stack compared to CMP stack sections. Moreover, the CRS stack parameters obtained during the stack form the foundation for a robust reflection tomography used for velocity model building. These models allowed the application of pre-stack and post-stack depth migration. The obtained depth images provided structural details not seen before, motivating an alternative view on the structural setting of the area. The image of the Jurassic salt plug indicates tectonics similar to observations in the Allertal region, where reverse faulting plays a major role in the evolution of the salt structures. As a consequence, shortening of the Mesozoic strata was included into the revised interpretation of the Glueckstadt Graben area. The new depth images also allowed an updated look on the petroleum system of this graben, which indicates new possible exploration targets.

INTRODUCTION

Salt plugs and their structural development represent a dominant part in the subsurface of northern Germany (Fig. 1). Many commercial applications are linked to the effects of salt tectonics, e.g. salt plugs are a source of raw material for different salts and many oil accumulations are closely associated with the development of salt plugs (Boigk, 1981). Limestone mining would not be possible in the region of Schleswig-Holstein in northern Germany if salt plugs had not lifted Upper Cretaceous sediments to the surface of the earth (Laegerdorf quarry near the City of Glueckstadt). Moreover, gas deposits were explored at the base of salt plugs (see Pasternak, 2006). Salt plugs have contributed to the appearance of the landscape in the past ("Kalkberg" near the City of Segeberg, Schleswig-Holstein, the Island of Helgoland within the southern North Sea, a.o.). Even today, direct and indirect indications of their existence can still be seen at the surface of the earth and some effects, like the development of sink holes, might be hazardous in urban areas.

The functional dependence of the individual northern German salt structures on salt stock families (Fig. 1 and Fig. 2) was outlined by Sannemann (1968) and their history was described by Jaritz (1973). Trusheim (1957) introduced the term halokinesis. In the explanations of the formation of salt plugs and the development of salt plug families these authors presumed density instabilities for the North German area between underlying light salt und overlying heavy sediments to be the major force of the buoyancy driven

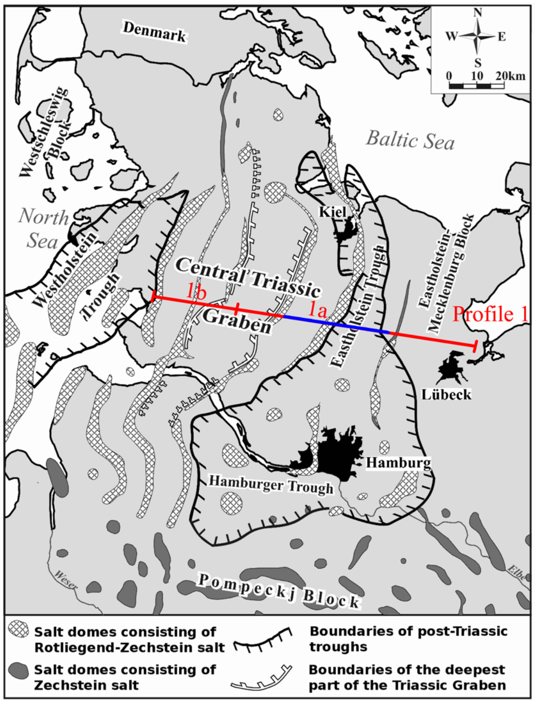

Figure 1: Map of Northern Germany displaying major geological units and cities as well as the distribution of salt stock families and salt plugs, modified after Maystrenko et al. (2005). The Central Triassic Graben is also known as the Glueckstadt Graben. The area of the eastern second generation salt plug is shown with a blue colour.

halokinetic processes. This assumption was already theoretically investigated in the early past by Hunsche (1978) and using analogue experiments by Heye (1978). There are new concepts of salt tectonics, e.g., by Hudec and Jackson (2007) for general concepts and Mohr et al. (2005) for NW Germany. However, for the particular area under investigation in this paper the evolution of salt stock families was not yet revisited. However, processing and interpretation of seismic reflection lines, gravity data, and density logs in boreholes raised severe doubts about the validity of this concept, at least for the early stages (i.e. Lower Triassic, Bunter) of the halokinesis in Northern Germany. Brink (1984, 1986, 1987) and Brink et al. (1992) reported several non-supporting observations of this concept:

1) Within the Northwest German Basin compressive "flower structures" were observed in seismic data at locations where previously salt plugs were assumed. This observation was further verified by drilling.

2) At the northern termination of the Glueckstadt Graben, a positive residual gravity anomaly at a location of a presumed salt plug had required a reinvestigation by modern seismic data and was finally proved to be a "flower structure" of Early Triassic times.

3) A salt plug in the Glueckstadt Graben centre, which was interpreted to be a member of the so-called "two-story" salt structures with a core of Rotliegend salt (Early Permian) and flanks of Zechstein salt (Late Permian) (see Baldschuhn et al., 2001), had to be redefined as a Late Triassic (Keuper) salt structure. What has happened to the Permian salt then? It should be noted here that no method is available so far to distinguish core samples of either Rotliegend salt or Keuper salt without any further information.

Due to these doubts concerning the role of the primary dome in the Glueckstadt Graben, salt domes of the second generation should be revisited as well (please note, that we use Trusheim (1957) notation to describe the location of salt plugs). In 2002, the industry provided seismic reflection data to the scientific

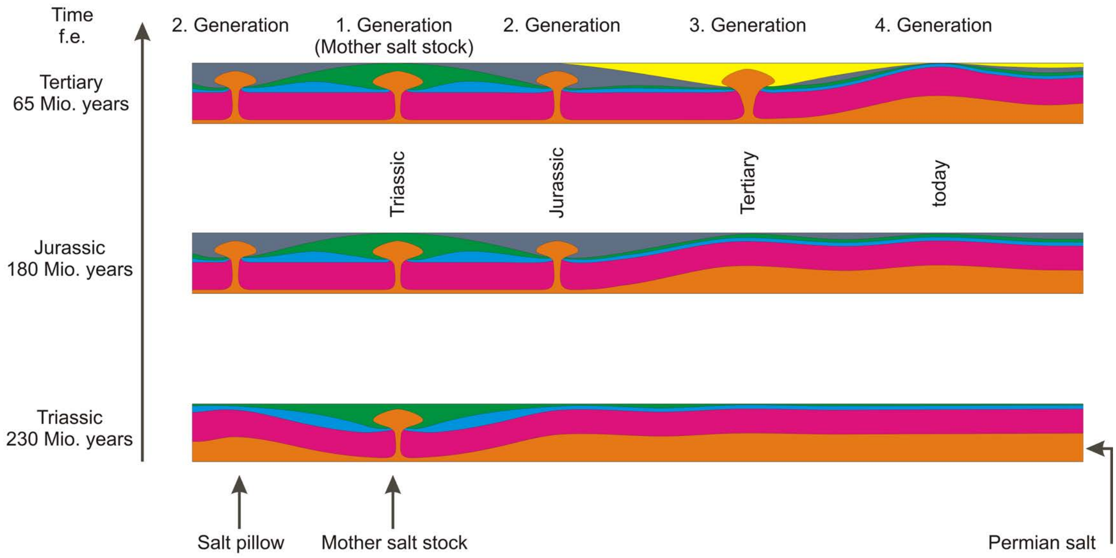

Figure 2: Concept of the evolution of a salt stock family, modified after Sannemann (1968).

community and opened new opportunities to have a more detailed look on the salt stocks of the Glueckstadt Graben area. Since these data were acquired in the 1980s they have a comparably low fold. New processing techniques like the CRS stack or the NIP (normal incidence point)-wave tomography which are particularly suited to improve the imaging potential of low fold data were not available when the data were initially processed. Yoon et al. (2007) have applied the CRS stack technique to these data with the focus on the imaging of the basement and lower crustal structures as well as Moho-topography.

In this paper the data are reprocessed with the emphasis on the salt plug families and the sedimentary structure. Also velocity model building and pre-stack as well as post-stack imaging is applied. Using the CRS stack the images of the data were considerably improved compared to the processing of the 1980s. The obtained velocity models and depth images in fact provide further evidence to question the classical concept of salt plug and salt stock family development in the Glueckstadt Graben area.

REPROCESSING OF SEISMIC DATA

The reflection seismic data which were provided to the scientific public in 2002 were acquired and processed in the 1980s. Compared to contemporary reflection acquisitions, the fold of these data is low (about 20). The processing in the 1980s provided basically stacking velocities and the Common Midpoint (CMP) stacks. Velocity model building, time and depth migration was usually not applied to these data. Due to the structural complexity combined with the low fold, severe imaging challenges were met.

The CRS stack technique provides a contemporary processing tool to enhance the image quality of these data. The CRS stack is best suited to cope with low fold data since a physically reasonable formation of super bins where the dip of the structure is included is the basic principle of this method. The larger number of traces in these bins leads to an improved signal-to-noise (SN) ratio, when compared to the classical CMP processing.

CRS stack and NIP-wave tomography

The CRS stack is a multi-parameter stacking technique. The traveltime t of reflection events (Eq. 1) is described by three parameters A, B, and C instead of one parameter V_{nmo} for the classical CMP stack (Eq. 2) (see e.g. Mann, 2002; Mueller, 1999). In the Eq.s X is the source-receiver offset, m is the midpoint offset with respect to the considered CMP position and t_0 corresponds to the zero offset (ZO) two-way traveltime (TWT). A, B, and C as well as V_{nmo} are stacking parameters of the CRS and CMP stack, respectively.

$$t^2[m,X] = (t_0 + Am)^2 + t_0(Bm^2 + CX^2) \tag{1}$$

$$t^2(X) = t_0^2 + \frac{X^2}{V_{nmo}^2} \tag{2}$$

The parameters A, B, and C are called CRS stack parameters or CRS stack attributes. Both stacking formulas represent short spread hyperbolic traveltime approximations. Practically this means X has to be reasonably small in order to satisfy this condition. No assumption on the model is required to derive the formulas. They are applicable to any kind of heterogeneous model. This is the major reason why stacking is such a stable procedure in seismic data processing. The CMP stack is a subset of the more general CRS stack. If the midpoint offset m is zero we immediately transform Eq. 1 into Eq. 2 with $V_{nmo}^2 = \frac{1}{t_0 C}$. The incorporation of the midpoint offset into the CRS stack results in the construction of super bins where the dip of reflectors is included through parameter A. Due to this the CRS super bin is superior to just merging several CMPs where the dip of the structure is not considered.

Depending on the CMP offset m, the CRS super bin contains a considerable larger number of traces than the CMP gather. The CRS stack therefore shows a much improved SN ratio when compared to the CMP stack. The choice of the midpoint offset m is important for the resulting lateral resolution of the CRS stacked section. The size of the first Fresnel zone is a good guidance for this parameter which can be interpreted as the lateral extension of the super bin. In this case the lateral resolution of CRS and CMP stack is the same.

The implementation of both stacks works along similar schemes. Prior to the stack the stacking parameters need to be determined. In the CMP stack V_{nmo} is scanned by testing a certain parameter range and choose its optimum value by evaluating a coherence measure like the semblance. This process is usually described as stacking velocity analysis. A similar approach is applied in the CRS stack; here, however, we have to perform coherency scans to fit three parameters simultaneously, which is more costly. Instead, three one-parameter searches are implemented. The CRS stack enhances all coherent events present in the data, e.g., also multiples and diffractions. If multiples have hyperbolic moveout, they are well approximated by the CRS stack operator, and the stacking parameters for these events will be determined during the search procedure. However, multiples with moveouts that deviate significantly from the moveouts of neighbouring primary events can be attenuated by introducing a reference model of stacking velocities to the CRS stack sequence (e.g. Mueller, 1999). Using this so-called constrained CRS stack reduces the computational time and further improves the image quality of the CRS stack in general (e.g. Yoon et al., 2007).

The moveout velocity in the CMP stack is usually assumed to be the stacking velocity. In case of an arbitrary medium V_{nmo} is a processing parameter. Only for the case of a horizontally stratified medium the stacking velocity can be transformed into the physical parameter interval velocity via Dix inversion. The CRS stack parameters A, B, and C can be considered as processing parameters as well. If Eq. 1 is rewritten in a different parameterisation (Eq. 3), the parameters can be interpreted physically, which is important for subsequent velocity model building and depth imaging.

$$t^2[m,h] = (t_0 + \frac{2sin\alpha}{V_0}m)^2 + \frac{2t_0 cos^2\alpha}{V_0}(\frac{m^2}{R_n} + \frac{h^2}{R_{nip}}) \tag{3}$$

Here, α is the angle of emergence, V_0 is the near surface velocity, R_n and R_{nip} are radii of curvature of the normal (N) wave and normal-incidence-point (NIP) wave, respectively, and h is half source-receiver offset, i.e., $h = \frac{X}{2}$. The N- and NIP-waves are generated by two hypothetical one-way experiments (Hubral, 1983). The NIP-wave is generated by a point source on the reflector where the source position is given by the ZO ray of the considered CMP. The N-wave is generated by an exploding reflector element centred around the ZO ray. These wavefield attributes or CRS parameters can be used to determine a smooth, laterally inhomogeneous subsurface model for depth imaging. A detailed description of the tomographic approach using the CRS stack parameters which is called NIP-wave tomography is given in Duveneck (2004). With a correct velocity model, the NIP-wave, when propagating back to the subsurface, should focus at its hypothetical source location at zero traveltime. Based on this criterion, an optimum velocity model is found iteratively by minimizing the misfit between the measured and modelled wavefield attributes of the input data. Since reflection points are treated independently of each other, only locally coherent events in the CRS stacked data are required and very few picks are needed for the tomographic inversion. As a smooth model description is used by the technique, it is not necessary to pick the reflection events continuously. The picking is performed in the CRS stacked domain with its high SN ratio either manually or in automatic mode with respect to the certain threshold and semblance settings. The quality of ZO picks is controlled during the inversion procedure. After every iteration, the locations of back-propagated depth converted input picks are computed, and displayed together with the velocity model to visually control the distribution of the picks.

THE DATA

The reprocessed profile 1 is located north of the river Elbe which almost coincides with the so called Elbe lineament and crosses the Central Triassic Graben and its deepest part, i.e., the Glueckstadt Graben, perpendicular to the graben axis (Fig. 1). Profile 1 was acquired during two field campaigns. The eastern part (profile 1a) consists of 771 shot gathers with a mean shot point spacing of 120 meters. In total 120 channels were used to record each shot with a geophone spacing of 40 m, providing maximum offsets of 4800 m. The total recording time was 13 s. The second part of profile 1 (profile 1b) was recorded as a western extension of the first acquisition and comprises 553 shot gathers with a recording time of about 13.3 s. Explosive sources were used for both parts of the profile 1. In this study, which focusses on the sedimentary structure and salt features, we consider up to 6 s TWT. Some preprocessing was applied to the data to enhance the quality and SN ratio. The preprocessing sequence started with setting up the field geometry and applying the field static provided with the data. Then, manual trace editing was carried out, e.g. elimination of dead and noisy traces and high-frequency bursts in the shot gathers. After the trace editing, top muting was applied to remove the direct and refracted waves. Also bottom muting was used to eliminate the strong instrument noise present in some shot gathers at later times. The datasets were filtered using a bandpass filter of 5/18 to 45/50 Hz. The irregular shooting geometry leads to a varying CMP fold of about 20 for profile 1a and about 30 for profile 1b on average with a midpoint spacing of 20 m. For profile 1 in total 4649 (1a) and 1725 (1b) CMP gathers were obtained. In order to enhance the amplitudes of reflection signals at deeper levels, an automatic gain control (AGC) was applied to the CMP gathers. The time window of the AGC was 1000 ms. After applying the CMP and CRS stack, the sections were merged together resulting in a total profile length of about 120 km.

CMP and CRS stacking

Stacking of the data in the time domain was split into two major parts. In the first part the data were stacked by the classical CMP stack using the stacking velocities provided with the data. In the second part the datasets were processed with the CRS stack method.

For profile 1a stacking velocities provided with the data were used for CMP stacking. For its western extension (profile 1b) no information about stacking velocities was available, and conventional stacking velocity analysis at several CMP locations was performed. Stacking velocities for the western part of profile 1a were used as a guide during the analysis. The CMP stacked sections for both profiles are computed separately and merged together. This results in ca. 6000 CMPs along the combined section of about 120 km extension. The resulting CMP stacked section is shown in Fig. 3 down to 6 s TWT.

The CRS stack was applied to the preprocessed CMP gathers. The most crucial parameters of the automatic CRS stack are the stack apertures represented by parameters X and m (see equations above). After a number of experiments, the offset X was defined between 2000 m for near-surface times to 4945 m, i.e., full acquisition aperture, at about 5 s TWT. The interpolation of the aperture in between is linear, whereas for later times the maximum available aperture was used. The midpoint offset m is defined in the time-midpoint domain of the ZO section. In order to image near surface structures as well as deeper structures properly, different apertures were tested. Finally, the midpoint offset was defined between 400 m at the near-surface to 2000 m at 5 s TWT. The latter midpoint offset aperture was also used at later times. These values correspond approximately to the size of the first Fresnel zone for the considered areas. The stacking fold for the CRS stack is between 400 and more than 2000, i.e., an increase of up to two orders in magnitude compared to the CMP fold.

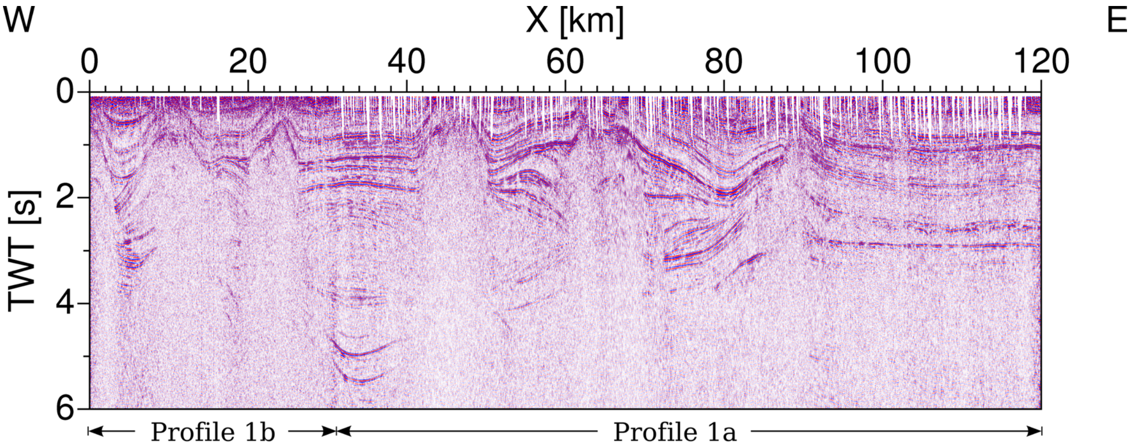

Figure 3: CMP stack of profile 1. Salt plugs are between 8 and 15 km (3rd generation west), 20 and 27 km (2nd generation west), 40 and 50 km (1st generation, mother salt plug), 60 and 70 km (2nd generation east) and 80-90 km (3rd generation west) in lateral direction.

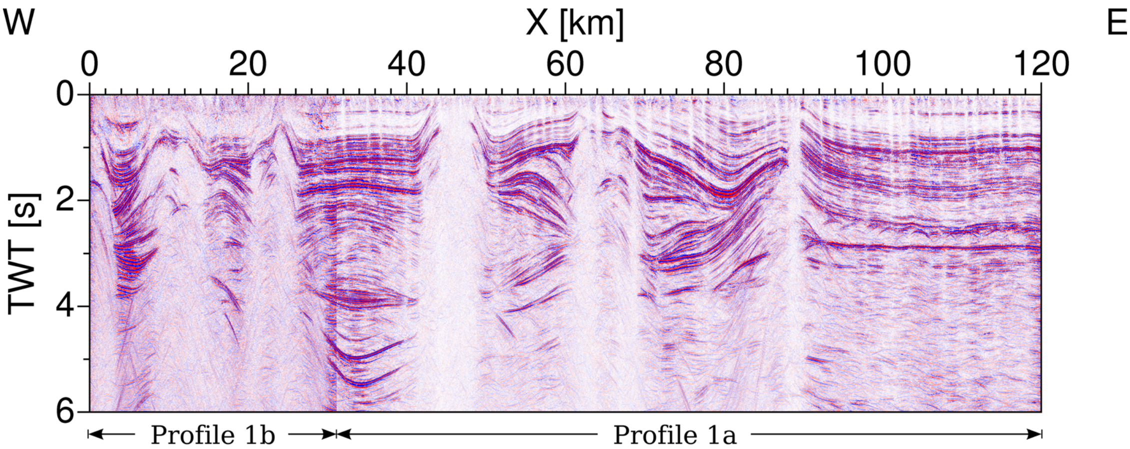

Figure 4: CMP stack of profile 1. Salt plugs are between 8 and 15 km (3rd generation west), 20 and 27 km (2nd generation west), 40 and 50 km (1st generation, mother salt plug), 60 and 70 km (2nd generation east) and 80-90 km (3rd generation west) in lateral direction.

For profile 1 the stacking velocities provided with the dataset and obtained by velocity analysis were applied to build the reference velocity models in the CRS stack. Velocity values obtained from the conventional stacking velocity analysis were linearly interpolated for every CMP location and every time sample of the stacked section. Resulting velocity sections were used for the constrained CRS stack and guided the CRS parameter search. Both profiles 1a and 1b were separately processed and merged together resulting in the CRS stacked section shown in Fig. 4.

The stacking results

CMP and CRS stacked sections

The CMP section of profile 1 (Fig. 3) provides a very detailed image of the sedimentary part down to 3 s TWT as well as of the salt plugs between 8 and 15 km (3rd generation west), 20 and 27 km (2nd generation west), 40 and 50 km (1st generation), 60 and 70 km (2nd generation east) and 80 and 90 km (3rd generation east) in lateral direction (Fig. 3). At 88 km, a steep fault is visible, which separates the East-Holstein Trough in the west from the East-Mecklenburg block in the east (Maystrenko et al., 2005).

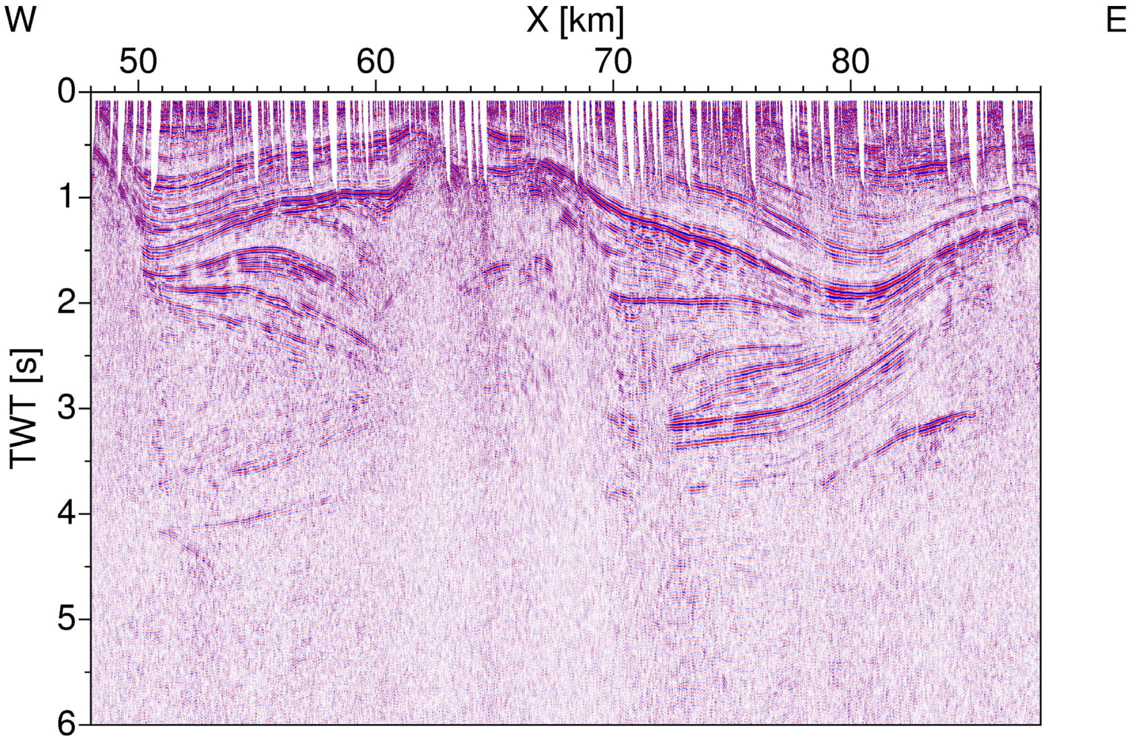

Figure 5: CMP stack of the eastern second generation salt plug.

Also, sharp parallel dipping reflections are observed in the upper crust between 4.5 and 5.5 s TWT (x = 30-40 km) that can be correlated with two parallel dipping reflections between 50 and 60 km at 3 to 4 s TWT. These reflections correlate with a high conductivity body observed in magnetotelluric data (e.g. Hoffmann et al., 2005).

Reflections are barely visible in the deeper parts. The comparison of the CMP stack section with the CRS stack section (Fig. 4) shows that the CRS stack significantly improved the SN ratio and generally improved the image quality. The image of the sedimentary cover as well as of internal salt structures is clearer and more detailed than in the CMP stack section. Also, between 90 and 120 km the reflections in the upper crust are enhanced.

The CRS stack significantly improved the images of the salt plugs. A direct comparison of the CMP and the CRS stack of the eastern second generation salt plug (Fig. 5 and Fig. 6) shows, that the reprocessed results display details of the salt interior not seen before. The CRS stack section shows apparently different reflectivity patterns in the eastern part than in the western part of the profile. The section reveals a comparably highly reflective upper crust within a 3 to 4 s wide band in the eastern part. This might indicated that this area was tectonically less active than the area in the western part of the profile 1a where less reflectivity is observed.

Velocity model building using NIP-wave tomography

All required information for the tomographic inversion is contained in the kinematic wavefield attributes obtained from the CRS stack. To acquire the input information for the tomography, a number of ZO points describing the primary events were selected. Once the CRS stack is performed and the CRS parameters are available, the picking of ZO points can be performed either manually or using an automated picking tool. A part of profile 1a, containing the second eastern generation salt plug, was processed with the NIP-wave tomography. In total, 2000 CMP gathers were processed, which corresponds to about 40 km of the profile (Fig. 6).

The automatic picking procedure is performed in the CRS stacked sections using a coherency criterion. In general, the quality of picks depends on the quality of stacked sections provided by the CRS stack.

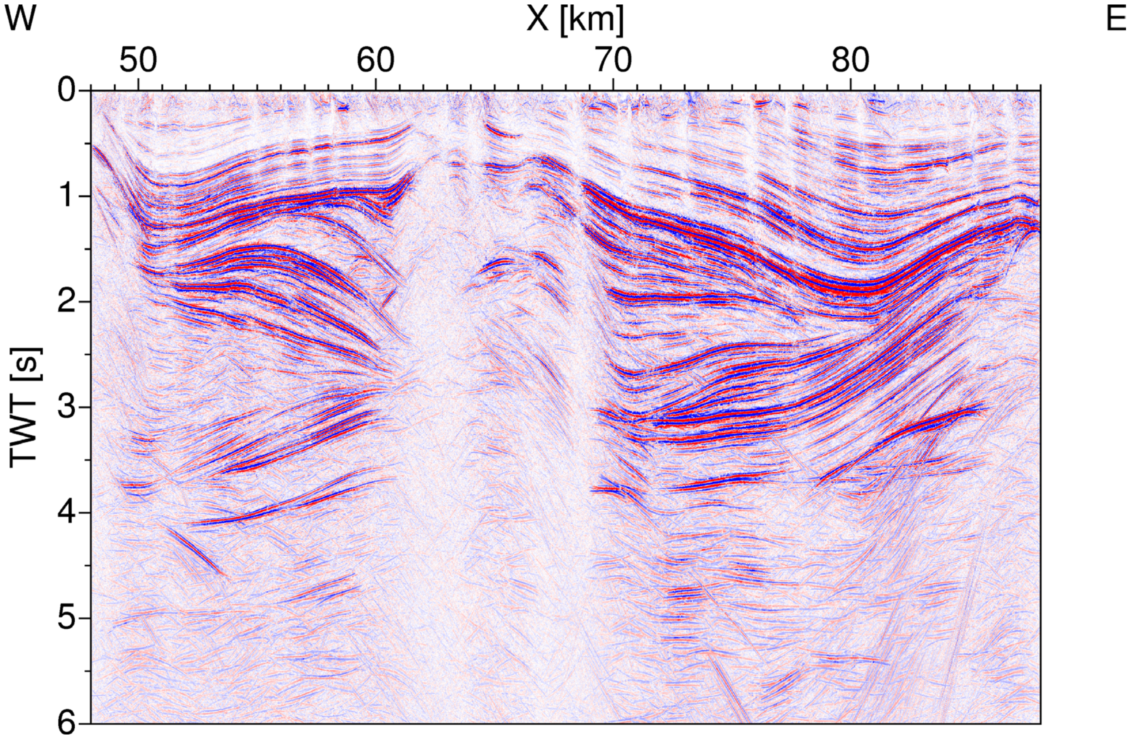

Figure 6: CRS stack of the eastern second generation salt plug.

Therefore, the proper choice of the CRS stack parameters, especially source-receiver and midpoint offset apertures (see Eq. 1, Eq. 3), is essential. The enhanced SN ratio of the stacked domain provides better reliability of the picks used for tomography than the pre-stack data. About 15000 picks were selected for the inversion (Fig. 7). The distribution of the picks is in good correlation with the main structures present in the section (Fig. 6). Strong seismic impedance contrasts at the main seismic boundaries provide high coherency values and, therefore, reliable results of the automatic picking down to the base Rotliegend. Moreover, even internal reflections in the eastern part of the salt body (x = 63-68 km, 1.5 - 2 s TWT) are picked properly and may be correlated with the main deposits present in the flanks of the structure. The kinematic wavefield attributes associated with the picked ZO points were automatically extracted from the CRS parameter sections.

The velocity model was determined on a grid of 41 x 41 knots in lateral and vertical direction, respectively. The horizontal knot spacing was 1000 m, the vertical knot spacing was 200 m. As an initial model a near-surface velocity of 1750 m/s with a constant velocity gradient of 0.5 s^{-1} was used. The gradient of 0.5 s^{-1} can be considered as a proper velocity gradient of the upper part of the sedimentary cover in this area. No a priori information about velocities like well logs was used for the tomographic inversion. With these parameters the inversion effectively converged after a total of 5 iterations. In areas without picks the final tomographic model usually reflects the starting model of the inversion. The final velocity model combined with the locations, where CRS parameters were picked and used for the tomographic inversion, is shown in Fig. 8. The velocity model and the distribution of migrated picks are consistent with the input data. High accuracy of the velocity model in areas with enough input picks was confirmed by the residual moveout control of depth-migrated common reflection point (CRP) gathers.

In the upper part of the section the tomographic model shows velocities varying between 1800-3500 m/s, which is typical for Tertiary sediments. At the depth level of 3000 m two local velocity maxima with velocities of about 4500 m/s are present at 64 km and 80 km in the section. These maxima might indicate salt accumulations or salt rich sediments. Areas with only a few picks (see Fig. 8) display little deviations from the initial velocity model, e.g., in the region of the internal salt structure (x = 68 km, 3-8 km depth), as well as in the eastern part of the section (x = 48-58 km, 3-5 km depth). Although there are some input

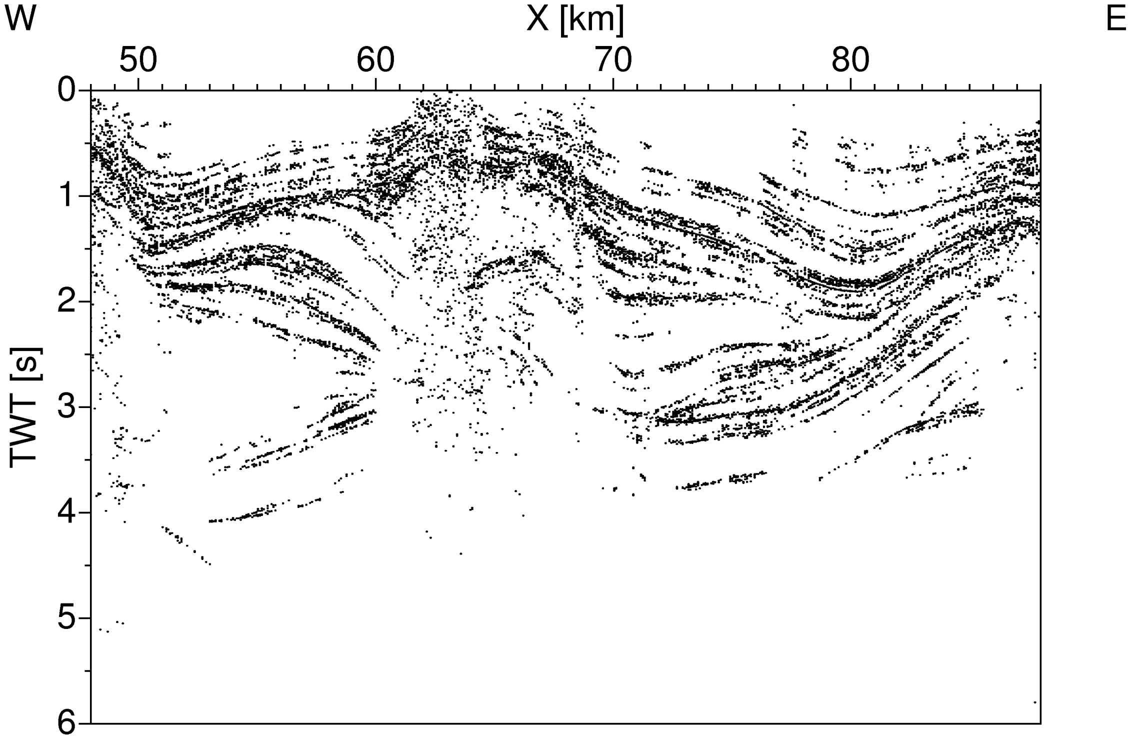

Figure 7: Locations of parameter picks used in the tomographic inversion.

picks available for the deeper parts of the section, the tomography did not converge well in this area, and the final model corresponds almost to the initial model. Along the edges of the model, i.e. between x= 48-53 km and x = 83-88 km, no reliable velocity information is available, due to the absence of appropriate ray paths in the tomography procedure. Further, those parts of the velocity model where only few or no picks exist, should not be included into the interpretation.

Depth migrated images

The velocity model obtained by the tomographic inversion was used to perform post-stack and pre-stack depth migration. Kirchhoff depth migration was applied to the CRS stacked section of Fig. 6 and to the pre-stack data. The results down to 10 km depth are displayed in Fig. 9 and Fig. 11, respectively. Zoomed interior of the salt structure is shown in Fig. 10. The depth sections provide additional details of the structural features of the second generation salt plug and its environment.

The eastern second generation salt plug, flanked by the secondary rim syncline of Jurassic age, shows a set of unique internal reflections. Quite often such internal reflections belong to anhydrite or carbonate floaters within salt plugs, but they seem to be different here. Similar reflections are also recorded within the second generation salt plug on the western side of the graben (Fig. 4).

Comparing the results of the CRS stack processing with the results of the seismic standard processing a significant difference of the seismic images is recognizable. The reprocessed depth images (Fig. 9 and Fig. 11) reveal new details and indicate an alternative geological interpretation of the salt structure and the underlying pre-Permian. The latter results in a new evaluation of the hydrocarbon systems in this area. This includes the structural setting as well as the distribution of source rocks, and possible migration pathways.

DISCUSSION

The Jurassic rim syncline is part of the East Holstein Jurassic Trough (see Fig. 1), which contains a commercial petroleum system based on the Early Jurassic Liassic Posidonia shale as source rock and the Middle

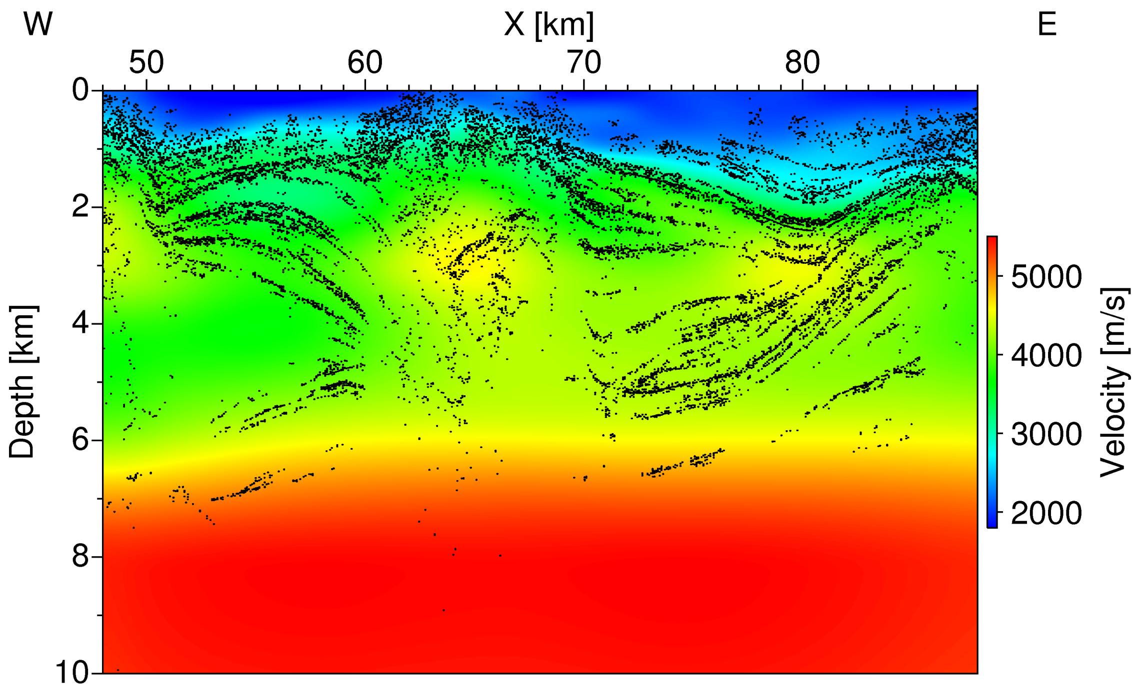

Figure 8: Tomographic velocity model with the locations of parameter picks used in the inversion.

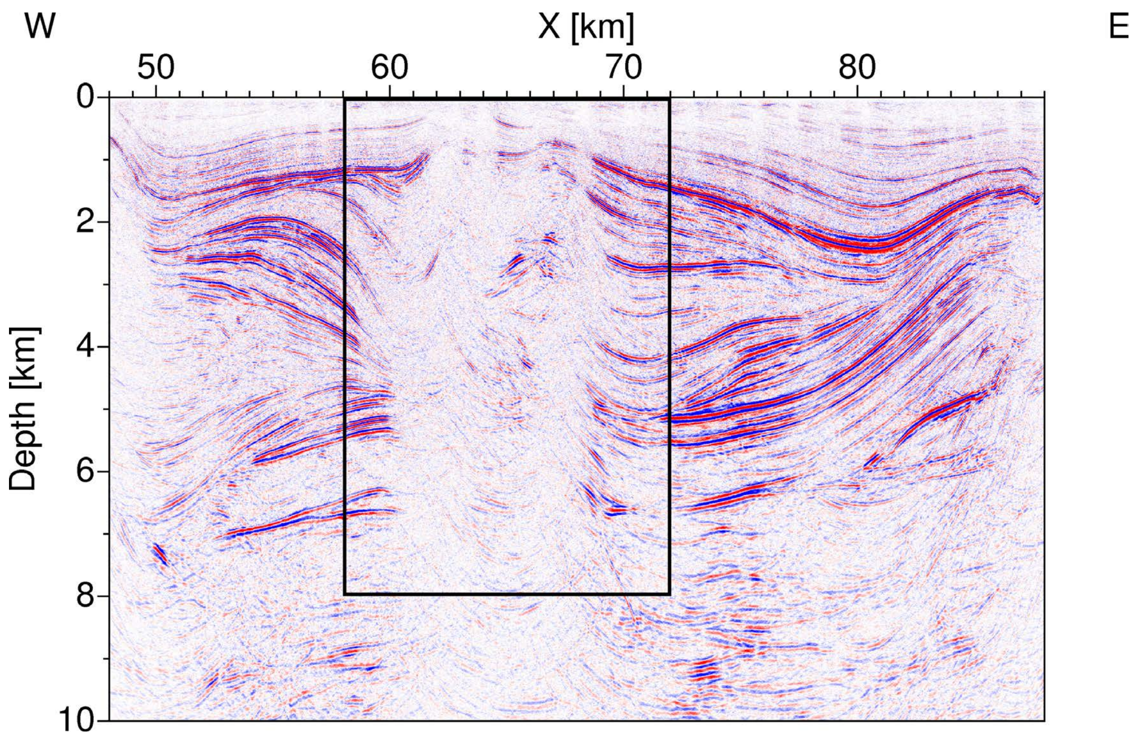

Figure 9: Post-stack depth migration of the CRS stack (Fig. 6) using the velocities from the tomographic inversion (Fig. 8). Zoom of the framed area is shown in Fig. 10.

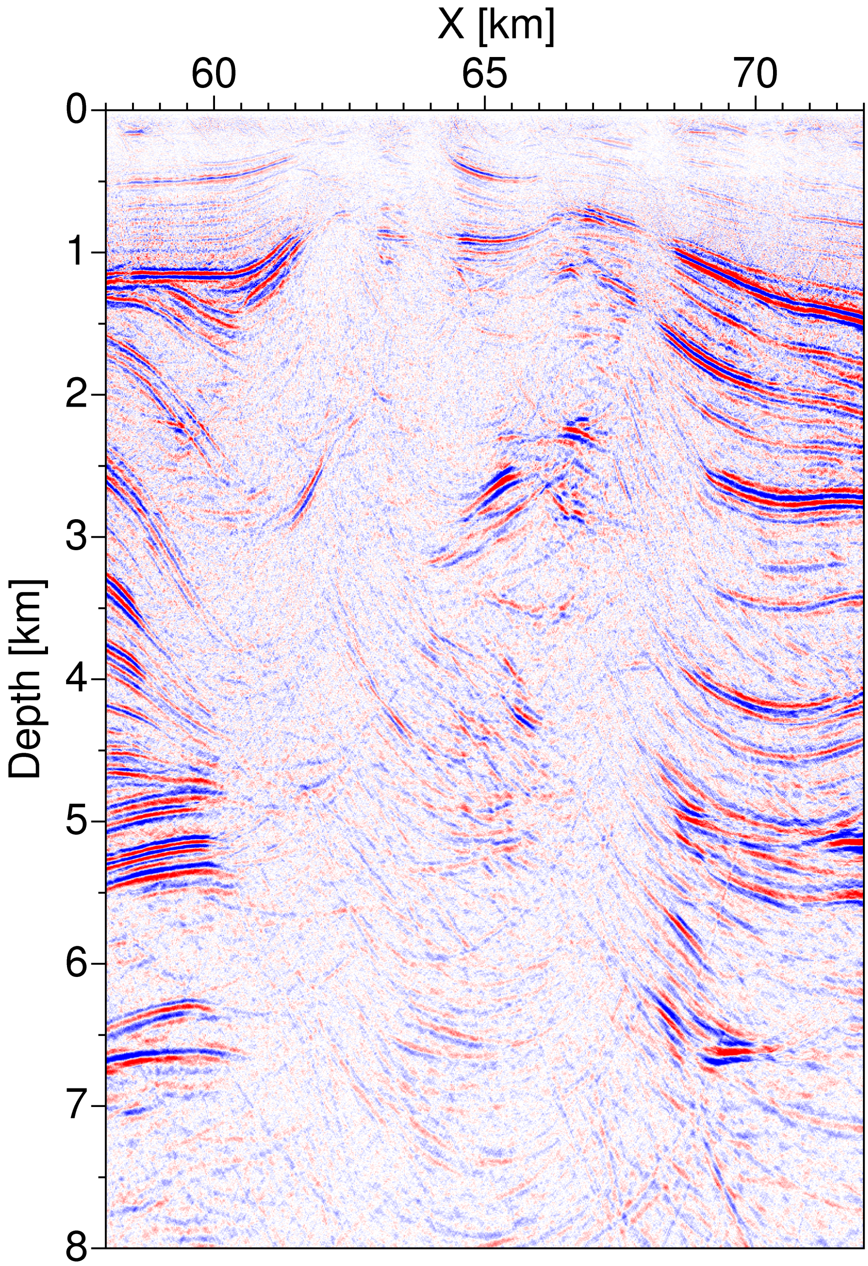

Figure 10: Post-stack depth migration of the CRS stack. Zoom of the Fig. 9.

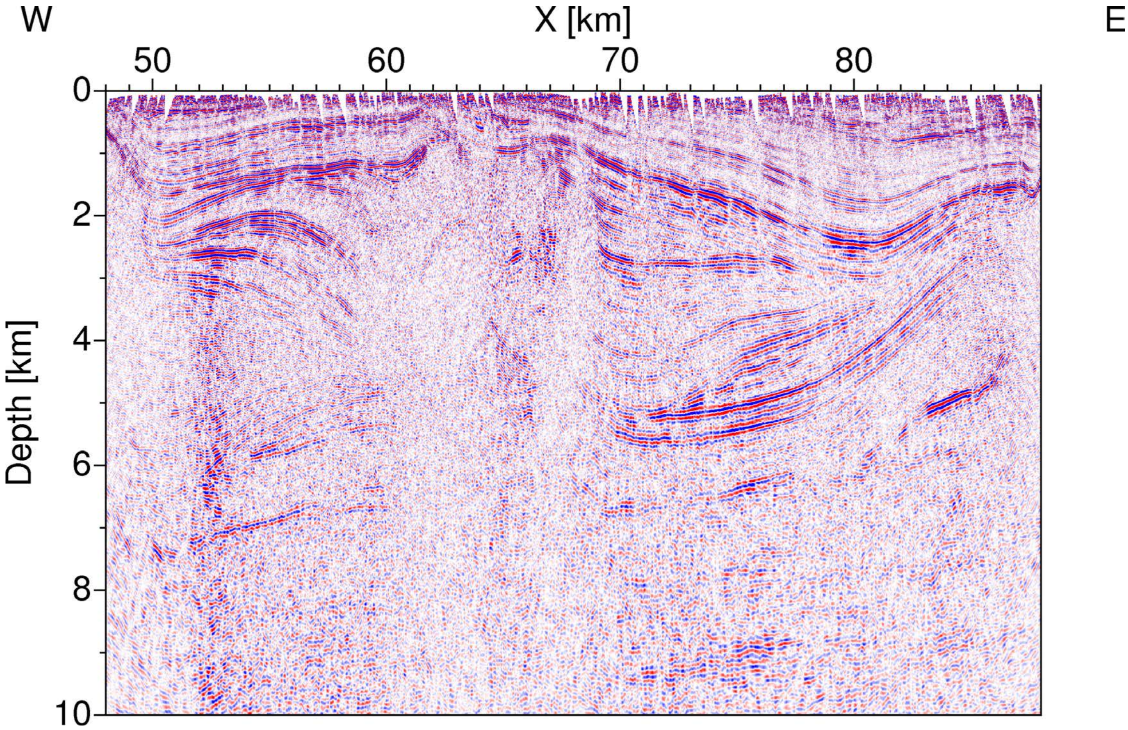

Figure 11: Pre-stack depth migrated section of the eastern second generation salt plug

Jurassic Dogger sandstones as reservoir rocks. Since the position of this trough coincides with gravity and magnetic highs, its development must have some relations to processes at greater depths (Brink, 1984). Therefore, in the chronological sequence and the spatial arrangement of the salt structures of the Glueckstadt Graben, tectonic processes may have interfered synergetically with halokinetic events and produced the complex pattern in the salt plug distribution. We discuss first the structural setting of the eastern second generation salt plug.

Structural setting

The reprocessed seismic depth image of the second generation eastern salt structure (Fig. 9 and Fig. 11) contains significant internal reflections, which appear to be different from the image of salt plugs commonly observed in the North German Basin. Instead, it shows significant similarities to features imaged by a seismic line crossing the Allertal regional tectonic lineament close to the city of Celle in the Lower Saxony Basin in the south of the Pompeckj Block (compare Betz et al., 1987; Mohr et al., 2005). In these images salt structures and overthrusts are tectonically associated. Both features developed predominantly during the inversion of the Lower Saxony Basin in Late Cretaceous to Early Tertiary times and define its northern fringe. The similar structural style supports the assumption of a similar tectonic evolution within the East Holstein Trough and the salt structures therein. However, the similarity does not include the same tectonic direction and an contemporaneous tectonic event. The thinning of the Tertiary layer on top of the structure certainly indicates that the inversion has a Tertiary component. But an earlier transpressional event during the Kimmerian inversion in Late Jurassic times cannot be excluded as well. The "pearl string" of smaller remnants of Late Jurassic deposits along the Elbe-lineament in Schleswig-Holstein (Baldschuhn et al., 2001) may indicate a Kimmerian contribution to the tectonic setting. As observed at the Allertal lineament, a complex 3-dimensional tectonic setting with extensional, compressional and transversal features can be expected. Since the tree-dimensionality requires 3D-seismics and 3D-modelling techniques, the value of the presented 2D-method is still acceptable, but somehow limited, too. An interpretation of the reprocessed seismic depth section based on the concept of thrusting is displayed in Fig. 12. In such a structural setting

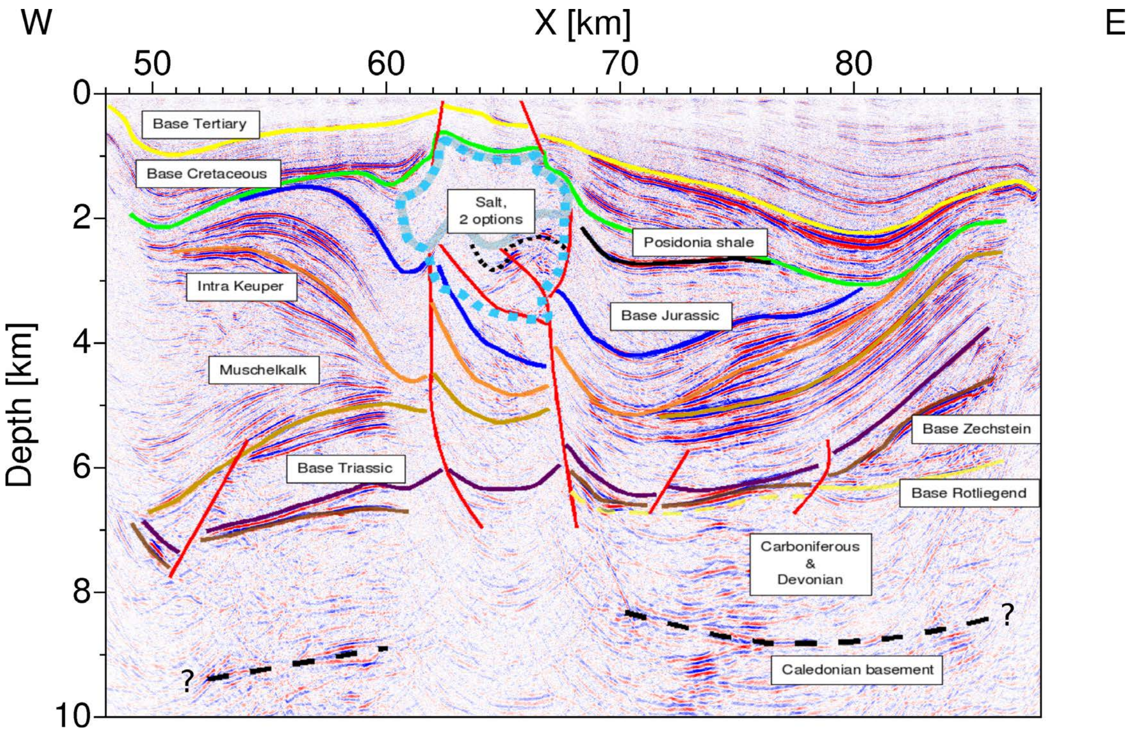

Figure 12: Post-stack migrated CRS section (Fig. 6) with interpretation. Interpreted horizons have been taken from published data (Bachmann and Grosse, 1989; Brink et al., 1992; Maystrenko et al., 2005). Horizon picks are well bore controlled.

with transversal movements and lateral salt flows 2D-balancing techniques, which may particularly support 2D-seismic interpretation results, are of limited value and have not been applied. Since one interpreted seismic line is not enough for a regional interpretation of the overall tectonics and the evaluation of a conjugate shear system, more seismic lines should be investigated.

Two west-vergent, steep faults are interpreted, which are located below a salt body with salt of unknown age (Rotliegend, Zechstein, Keuper?). This limited distribution of (shale and/or anhydrite rich) salt within the feature will not result in a well defined Bouguer gravity low. A salt rich feature was modelled by Yegorova et al. (2007) in a 2D-gravity study, resulting in a poor fit of observed and modelled data (Fig. 13). This poor fit may be caused either by an inadequate shape of the investigated salt bodies, especially of the reprocessed feature, or by an inadequate density distribution within the Mesozoic strata and below, or by the complex three-dimensionality of the feature, or all together. The present interpretation does not mean that the entire about 100 km long salt structure is similarly composed. However, the evidence of compressional tectonics is striking and a shortening of the Mesozoic strata of about 10% is possible, since the lateral length of base Cretaceous is correspondingly larger than the one of base Tertiary across the salt feature.

Shortening within the upper layers must have had an accompanying effect within the basement as well. Either an upthrusting within the basement took place, decoupled from the Mesozoic by the Permian salt layers, or metamorphic processes within the crustal rocks and associated shrinkage of rock volumes due to the pressure increase occurred. A combination of both processes is also possible. Upthrusting of basement rocks can certainly lead to positive magnetic and gravimetric anomalies as observed. On the other hand, according to Petrini and Podladchikov (2000), in regions exposed to horizontal shortening pressure gradients twice the lithostatic pressure can be achieved. This may result in an appropriate metamorphism of greenshist facies into eclogite facies if conditions of the middle crust are assumed. The density of the affected rocks will then increase from about 2.7 gr/cm^3 to about 3.4 gr/cm^3 and the rock volumes will decrease. This will result into a positive gravimetric anomaly as well as into a positive magnetic anomaly

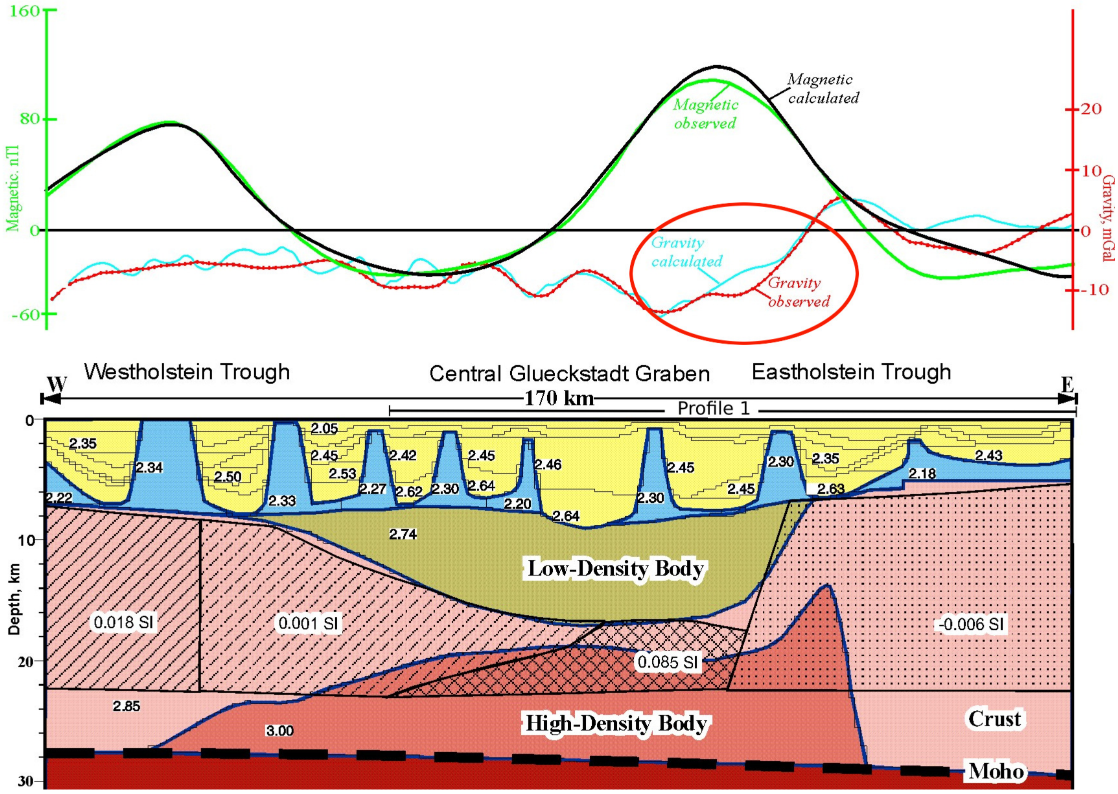

Figure 13: 2D Gravity model of the Glueckstadt Graben modified after Yegorova et al. (2007). Note the trade-off between the calculated and the observed gravity.

for rocks above the Curie depth. Since the gravimetric and magnetic highs are more or less coincident with the location of the Jurassic East Holstein Trough, a volume reduction within deeper crustal levels and the subsequent burial of the overlying strata appears to be more realistic than thrusting of the basement. The burial of the trough took place prior to the Kimmerian inversion in Late Jurassic times, when large amounts of Jurassic to Triassic strata were eroded on the adjacent areas. This burial was accompanied by reverse faulting of the Mesozoic strata, associated with the movement of salt. In Tertiary times, inversion processes occurred again and the structure became additionally overprinted.

This structural interpretation is supported by the seismic velocity distribution within the feature (Fig. 14). The dip of a low velocity channel is concordant with the dip of the interpreted thrust sheets. The magnitude of velocities indicates rather low velocity sediments instead of a high velocity salt body. The high velocity body at a depth of about 3 km within the centre of the salt complex and the thrust features may be part of the overlying salt body. In this case a high content of anhydrite may result in relatively higher velocities. Since light salt and heavy anhydrite are balancing each other, the resulting gravity effect may be insignificant as observed.

Distribution of source rocks

Within the Northwest German Basin two major source rocks - the base elements of the related hydrocarbon systems - are widely distributed. The first ones are Early Jurassic (Liassic) Posidonia shales (Binot et al., 1993) and the second ones are the Carboniferous coals (Cornford, 1998) and black shales (Gerling et al., 1999). Within the East Holstein Trough the Posidonia shale is charging the Dogger sandstone structures below the Lower Cretaceous unconformity at the flank of the "salt structure" and at distal positions of the secondary rim syncline. It is remarkable that within the realm of the "salt structure" seismic reflections have been recorded, which show a similar response like the Posidonia shale of the East Holstein Trough

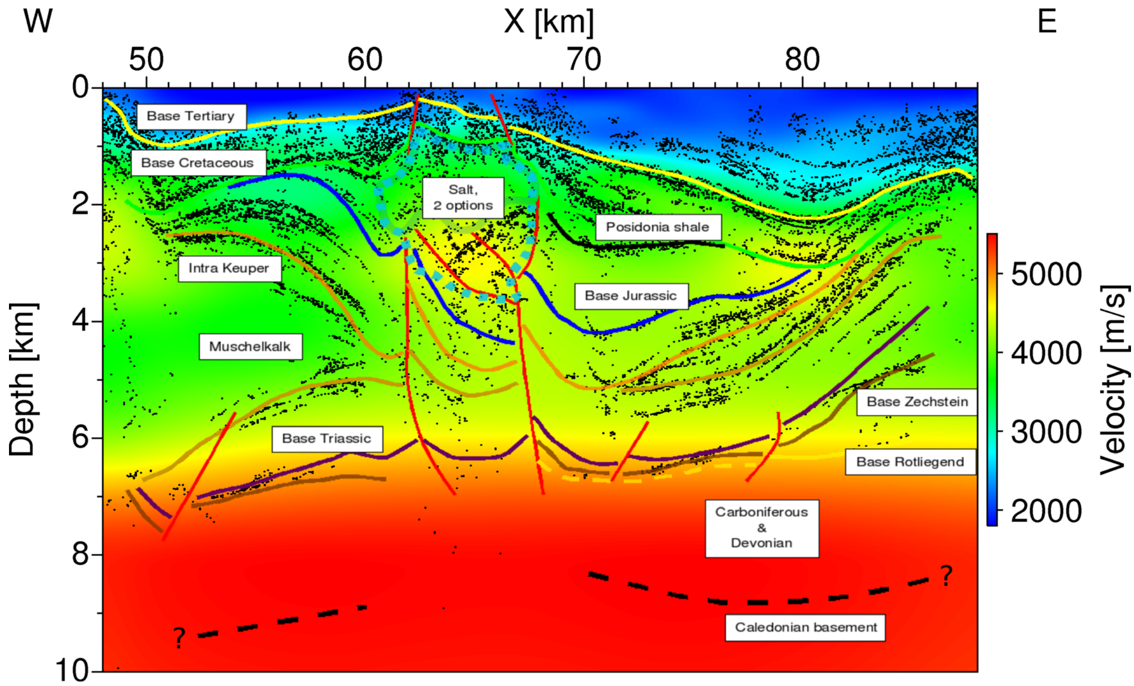

Figure 14: Tomographic velocity model (Fig. 8) with interpretation.

proper. It can at least be speculated that this source rock may also be present below the remaining salt body in the upper central part of the "salt structure". Whether Dogger reservoirs exist in a structurally high position within the structure, is even more speculative.

So far Upper Carboniferous coals were not penetrated by drilling within the area of Fig. 1. However, a well which tested the Triassic "flower structure" in the northern part of the Glueckstadt Graben, verified the presence of Lower Carboniferous black shales. This observation and the interpretation of magnetotelluric (MT) data (Hoffmann et al., 2005) support the assumption that electrically conductive and highly coalified Carboniferous source rocks may be widely present within the Glueckstadt Graben. The MT data were recorded at 10 locations along an East-West oriented profile across the total width of the graben. The central Glueckstadt Graben is characterized by a good conductor at a depth of approximately 10 km which is missing on the adjacent graben flanks.

For the first time significant pre-Permian seismic reflections have been well imaged in this study in shallower parts of the graben. These events could be indicative for the presence of coals and black shales within the pre-Permian strata. In the centre of the graben at very deep levels these reflections were already identified in the images obtained by former processing (Dohr, 1989; Bachmann and Grosse, 1989; Brink et al., 1992). However, within the deepest parts of the graben this potential source rock is certainly overmature since Triassic times. This may not be the case below the eastern flank of the East Holstein Trough, where the pre-Permian strata subsided still in Tertiary times and may then have entered and passed the gas generation window. The exact timing depends on the amount of Permian salt, which migrated away from this position into the eastern third generation salt plug, leaving a Tertiary rim syncline behind. As a rough estimate 1 km burial can be allocated to the salt migration, and about 1 km to tectonic subsidence.

Migration pathways

A third important and new observation of the reprocessed seismic line is the presence of faults at 72 and 78 km lateral position (see Fig. 12), which cut through the Early Triassic Bunter sequence at a position, where Rotliegend and Zechstein salts appear not to be present anymore. This observation supports the existence of migration pathways from the mature Carboniferous source rock into the sandstones of the Bunter as necessary requirement for charging post-Permian closures (Brink, 2002; Karnin et al., 2006).

Bunter structures, which were drilled in this area so far, are mainly anticlinal features above Permian salt pillows. Under these circumstances, the Permian salt acts as a perfect seal and migration of hydrocarbons were severely hampered.

CONCLUSION

The presented results of seismic reprocessing using the CRS stack technique leads to revised considerations of the structural setting and the evolution of salt plugs in the area of the Glueckstadt Graben. The reprocessing of the data provided by the hydrocarbon industry clearly demonstrates the capabilities of the CRS technique for low fold data. The images display a considerably improved SN ratio and show much more details than the CMP processing of the 1980s. Moreover, a velocity model consistent with the data was build and used to perform pre- and post-stack depth migrations which were so far not available for these data. The image of the Jurassic salt plug indicates tectonics similar to observations in the Allertal region, where overthrusting plays a major role in the evolution of the salt structures. As a consequence shortening of the Mesozoic strata was included into the revised interpretation. The reprocessing provided also new insights into the petroleum system in this area indicating new possible exploration targets.

The presented results may lead to a new view of the geological understanding of the area. Instead of a "two-story-salt plug", steep reverse faults and associated salt structures similar to the features along the Allertal-Lineament may have to be assumed for the location of the investigated seismic line. Based on this interpretation previous studies (e.g. Baldschuhn et al., 2001; Maystrenko et al., 2005) may have to be revised if the presented results are further constrained by ongoing studies at the western second generation salt plug.

ACKNOWLEDGMENTS

We are grateful to the German Research Foundation (DFG) for supporting this project (Ga 350/12) through the priority program SPP 1135 (Dynamics of Sedimentary Systems). The data were kindly provided by the Wirtschaftsverband Erdoel- und Erdgasgewinnung (WEG) through the technical management of the German Society for Petroleum and Coal Science and Technology (DGMK). We are also grateful to the Wave Inversion Technology (WIT) consortium for providing the CRS stack and NIP-wave tomography software. Discussions with Christian Huebscher and Stefan Duemmong are appreciated. We also thank Dr. Yuriy Maystrenko and Dr. Charlotte Krawczyk from the GFZ Potsdam and Dr. Bert Clever from Wintershall Noordzee B.V. for careful reading and reviewing the manuscript and making important and useful comments and suggestions.

REFERENCES

Bachmann, G. and Grosse, S. (1989). Struktur und Entstehung des norddeutschen Beckens - geologische und geophysikalische Interpretation einer verbesserten Bouguer-Schwerekarte. *Niedersaechsische Akademie der Wissenschaften*, Heft 2, 23-47, Anlage 3.

Baldschuhn, R., Binot, F., Fleig, S., and Kockel, F. (2001). Geotektonischer Atlas von Nordwest-Deutschland und dem deutschen Nordsee-Sektor - Strukturen, Strukturentwicklung, Palaeogeographie. *Geologisches Jahrbuch*, Band A 153.

Betz, D., Fuehrer, F., Greiner, G., and Plein, E. (1987). Evolution of the Lower Saxony Basin. *Tectonophysics*, 137:127–170.

Binot, F., P., G., Hiltmann, W., Kockel, and F., Wehner, H. (1993). The Petroleum System in the Lower Saxony Basin. *Special Publication of the European Association of Petroleum Geoscientists No.3*.

Boigk, H. (1981). Erdoel und Erdoelgas in der Bundesrepublik Deutschland. *Enke-Verlag*.

Brink, H. (2002). Halbwertszeiten im Kohlenwasserstoffhaushalt. *Erdoel Erdgas Kohle*, 2.

Brink, H.-J. (1984). Die Salzstockverteilung in Nordwestdeutschland. *Geowissenschaften in unserer Zeit, 2. Jahrgang*, 5:160–166.

Brink, H.-J. (1986). Salzwirbel im Untergrund Norddeutschlands. *Geowissenschaften in unserer Zeit, 4. Jahrgang*, 3:81–86.

Brink, H.-J. (1987). Salzwirbel oder instabile Dichtebeschichtung? *Geowissenschaften in unserer Zeit, 5. Jahrgang*, 4:144–145.

Brink, H.-J., Duerschner, H., and Trappe, H. (1992). Some Aspects of the Late- and Post-Variscan Development of the NW-German Basin. *Tectonophysics*, 207:65–95.

Cornford, C. (1998). Source rocks and hydrocarbons of the North Sea, in Glennie, K.W., ed., Petroleum geology of the North Sea - Basic concepts and recent advances. *London, Blackwell Scientific Publishers*, pages 376–462.

Dohr, G. (1989). Ergebnisse geophysikalischer Arbeiten zur Untersuchung des tieferen Untergrundes in Norddeutschland. *Niedersaechsische Akademie der Wissenschaften*, Heft 2, Anlage 3:4–22.

Duveneck, E. (2004). Velocity model estimation with data-derived wavefront attributes. *Geophysics*, 69:265–274.

Gerling, P., Kockel, F., and Krull, P. (1999). Das Kohlenwasserstoff-Potential des Praewestfals im norddeutschen Becken - Eine Synthese. *DGMK-Forschungsbericht, Hamburg*, 433.

Heye, D. (1978). Experimente mit viskosen Fluessigkeiten zur Nachahmung von Salzstrukturen. *Geol. Jb.*, E12:31–51.

Hoffmann, N., Joedicke, H., and Horejschi, L. (2005). Regional Distribution of the Lower Carboniferous Culm and Carboniferous Limestone Facies in the North German Basin. - Derived from Magnetotelluric Soundings. *Z. dt. Ges. Geowiss.*, 156/2:323–339.

Hubral, P. (1983). Computing true amplitude reflections in a laterally inhomogeneous earth. *Geophysics*, 48(8):1051–1062.

Hudec, M. and Jackson, M. (2007). Terra infirma: Understanding salt tectonics. *Earth Science Reviews*, 82:1–28.

Hunsche, U. (1978). Modellrechnungen zur Entstehung von Salzstockfamilien. *Geol. Jb.*, E12:53–107.

Jaritz, W. (1973). Zur Entstehung der Salzstrukturen Nordwestdeutschlands. *Geol. Jb.*, A10:3–77.

Karnin, W., Gast, R., Baerle, C., Clever, B., Kuehn, M., and Sommer, J. (2006). Play types, structural history and distribution of Middle Buntsandstein gas fields in NW Germany: Observations and their genetic interpretation. *Z.dt.Ges.Geowiss., Schweizerbart'sche Verlagsbuchhandlung, Stuttgart*, 157/1:121–134.

Mann, J. (2002). Extensions and Applications of the Common-Reflection-Surface Stack Method. *Logos Verlag Berlin. ISBN 3-8325-0008-1. PhD thesis, University of Karlsruhe*, pages 2–52.

Maystrenko, Y., Bayer, U., and Scheck-Wenderoth, M. (2005). Structure and evolution of the Glueckstadt Graben due to salt movements. *Int J Earth Sci*, 94:799–814.

Mohr, M., Kukla, P., Urai, J., and Bresser, G. (2005). Multiphase salt tectonic evolution, in NW Germany: seismic interpretation and retro-deformation. *Int J Earth Sci*, 94:917–940.

Mueller, T. (1999). The Common Reflection Surface Stack Method: Seismic Imaging without Knowledge of the Velocity Model. *Der Andere Verlag, Bad Iburg. ISBN 3-93436-606-6. PhD thesis, University of Karlsruhe*, pages 9–36.

Pasternak, M. (2006). Exploration and Production of Crude Oil and Natural Gas in Germany in 2005. *Erdoel Erdgas Kohle*, 122, Heft 7/8.

Petrini, K. and Podladchikov, Y. (2000). Lithospheric pressure-depth relationship in compressive regions of thickened crust. *J. metamorphic Geol.*, 18:67–77.

Sannemann, D. (1968). Salt-stock families in northwestern Germany. In Braunstein, J. and O'Brein, G. D. (eds) Diapirism and Diapirs. *American Association of Petroleum Geologists, Tulsa, Memoir*, 8:261–270.

Trusheim, F. (1957). Ueber Halokinese und ihre Bedeutung fuer die strukturelle Entwicklung Norddeutschlands. *Z. Dtsch. Geol. Ges.*, 109:111–151.

Yegorova, T., Maystrenko, Y., Bayer, U., and Scheck-Wenderoth, M. (2007). The Glueckstadt Graben of the North-German Basin: new insights into the structure from 3D and 2D gravity analyses. *Int J Earth Sci*, in press.

Yoon, M., Baykulov, M., Duemmong, S., Brink, H.-J., and Gajewski, D. (2007). Reprocessing of seismic reflection data with the common reflection surface (CRS) stack method: New insights into the crustal structure of Northern Germany. *Tectonophysics*, revised.